



**HAL**  
open science

## Indirect X-ray photodesorption of $^{15}\text{N}_2$ and $^{13}\text{CO}$ from mixed and layered ices

Romain Basalgete, Daniela Torres-Díaz, Anne Lafosse, Lionel Amiaud, Géraldine Féraud, Pascal Jeseck, Laurent Philippe, Xavier Michaut, Jean-Hugues Fillion, Mathieu Bertin

### ► To cite this version:

Romain Basalgete, Daniela Torres-Díaz, Anne Lafosse, Lionel Amiaud, Géraldine Féraud, et al.. Indirect X-ray photodesorption of  $^{15}\text{N}_2$  and  $^{13}\text{CO}$  from mixed and layered ices. *Journal of Chemical Physics*, 2022, 157 (8), pp.084308. 10.1063/5.0100014 . hal-03752078v2

**HAL Id: hal-03752078**

**<https://hal.science/hal-03752078v2>**

Submitted on 19 Sep 2022

**HAL** is a multi-disciplinary open access archive for the deposit and dissemination of scientific research documents, whether they are published or not. The documents may come from teaching and research institutions in France or abroad, or from public or private research centers.

L'archive ouverte pluridisciplinaire **HAL**, est destinée au dépôt et à la diffusion de documents scientifiques de niveau recherche, publiés ou non, émanant des établissements d'enseignement et de recherche français ou étrangers, des laboratoires publics ou privés.

# Indirect x-ray photodesorption of $^{15}\text{N}_2$ and $^{13}\text{CO}$ from mixed and layered ices

Cite as: J. Chem. Phys. **157**, 084308 (2022); <https://doi.org/10.1063/5.0100014>

Submitted: 20 May 2022 • Accepted: 25 July 2022 • Accepted Manuscript Online: 25 July 2022 •

Published Online: 24 August 2022

 R. Basalgète, D. Torres-Díaz,  A. Lafosse, et al.



View Online



Export Citation



CrossMark

## ARTICLES YOU MAY BE INTERESTED IN

**Ammonia: The molecule for establishing  $^{14}\text{N}$  and  $^{15}\text{N}$  absolute shielding scales and a source of information on nuclear magnetic moments**

The Journal of Chemical Physics **157**, 084306 (2022); <https://doi.org/10.1063/5.0096523>

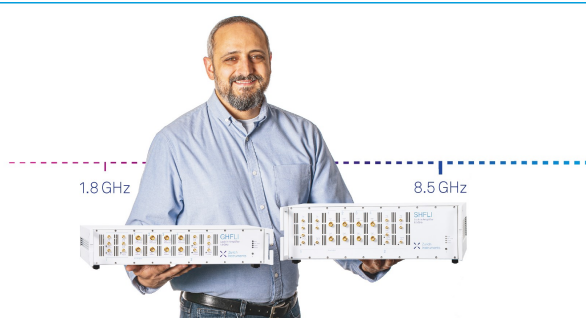
**Going beyond the electric-dipole approximation in the calculation of absorption and (magnetic) circular dichroism spectra including scalar relativistic and spin-orbit coupling effects**

The Journal of Chemical Physics **157**, 084120 (2022); <https://doi.org/10.1063/5.0094709>

**Helium droplet infrared spectroscopy of the butyl radicals**

The Journal of Chemical Physics **157**, 084311 (2022); <https://doi.org/10.1063/5.0102287>





**Trailblazers.** New

Meet the Lock-in Amplifiers that measure microwaves.

 Zurich Instruments [Find out more](#)

# Indirect x-ray photodesorption of $^{15}\text{N}_2$ and $^{13}\text{CO}$ from mixed and layered ices

Cite as: J. Chem. Phys. 157, 084308 (2022); doi: 10.1063/5.0100014

Submitted: 20 May 2022 • Accepted: 25 July 2022 •

Published Online: 24 August 2022



R. Basalgète,<sup>1,a)</sup> D. Torres-Díaz,<sup>1,2</sup> A. Lafosse,<sup>2</sup> L. Amiaud,<sup>2</sup> G. Féraud,<sup>1</sup> P. Jeseck,<sup>1</sup> L. Philippe,<sup>1</sup>   
X. Michaut,<sup>1</sup> J.-H. Fillion,<sup>1</sup> and M. Bertin<sup>1</sup>

## AFFILIATIONS

<sup>1</sup>Sorbonne Université, Observatoire de Paris, Université PSL, CNRS, LERMA, F-75005 Paris, France

<sup>2</sup>Univ. Paris-Saclay, CNRS, ISMO, 91405 Orsay, France

<sup>a)</sup> Author to whom correspondence should be addressed: [romain.basalgete@sorbonne-universite.fr](mailto:romain.basalgete@sorbonne-universite.fr)

## ABSTRACT

X-ray photodesorption yields of  $^{15}\text{N}_2$  and  $^{13}\text{CO}$  are derived as a function of the incident photon energy near the N ( $\sim 400$  eV) and O K-edge ( $\sim 500$  eV) for pure  $^{15}\text{N}_2$  ice and mixed  $^{13}\text{CO}:\text{N}_2$  ices. The photodesorption spectra from the mixed ices reveal an indirect desorption mechanism for which the desorption of  $^{15}\text{N}_2$  and  $^{13}\text{CO}$  is triggered by the photoabsorption of  $^{13}\text{CO}$  and  $^{15}\text{N}_2$ , respectively. This mechanism is confirmed by the x-ray photodesorption of  $^{13}\text{CO}$  from a layered  $^{13}\text{CO}/^{15}\text{N}_2$  ice irradiated at 401 eV on the N  $1s \rightarrow \pi^*$  transition of  $^{15}\text{N}_2$ . This latter experiment enables us to quantify the relevant depth involved in the indirect desorption process, which is found to be 30–40 monolayers in that case. This value is further related to the energy transport of Auger electrons emitted from the photoabsorbing  $^{15}\text{N}_2$  molecules that scatter toward the ice surface, inducing the desorption of  $^{13}\text{CO}$ . The photodesorption yields corrected from the energy that can participate in the desorption process (expressed in molecules desorbed by eV deposited) do not depend on the photon energy; hence, they depend neither on the photoabsorbing molecule nor on its state after Auger decay. This demonstrates that x-ray induced electron stimulated desorption, mediated by Auger scattering, is the dominant process explaining the desorption of  $^{15}\text{N}_2$  and  $^{13}\text{CO}$  from the ices studied in this work.

Published under an exclusive license by AIP Publishing. <https://doi.org/10.1063/5.0100014>

## I. INTRODUCTION

Diatomic molecules such as CO and  $\text{N}_2$  have been extensively studied in the laboratory at very low temperature ( $T < 20$  K), in their solid phase. Indeed, these molecules are expected to play an important role in astrophysical environments. For instance, they are observed directly (especially for CO) or indirectly (especially for  $\text{N}_2$ ) in the interstellar medium (ISM) and the solar system in a diversity of icy solids, such as interstellar ices (Boogert *et al.*, 2015), comets (Mumma and Charnley, 2011; Rubin *et al.*, 2015), and icy moons and planets (Owen *et al.*, 1993; Cruikshank *et al.*, 1993; Bennett *et al.*, 2013). Interaction of these icy solids with photons coming from nearby or distant stars can be at the origin of exchanges between solid and gas phases via the so-called photodesorption phenomenon. Photodesorption is a nonthermal process through which the energy of incident photons is absorbed by the ice and partly converted to the desorption of molecules

from its surface. In the last decades, it has been extensively studied in the vacuum ultraviolet (VUV) range (7–13.6 eV) for  $\text{N}_2$  and CO ices (Öberg *et al.*, 2007, 2009; Muñoz Caro *et al.*, 2010; Fayolle *et al.*, 2011, 2013; Bertin *et al.*, 2013).

More recently, the desorption induced by the irradiation of x rays, referred to as x-ray photodesorption, was also highlighted as a significant process for ices composed of simple (Dupuy *et al.*, 2018, 2021b) and complex molecules (Jiménez-Escobar *et al.*, 2018; Ciaravella *et al.*, 2020; Basalgète *et al.*, 2021a). More importantly, it was suggested that x-ray photodesorption of neutral molecules was strongly dependent on the ice composition via indirect desorption mechanisms (Basalgète *et al.*, 2021b). A detailed comprehension of these indirect processes on a microscopic scale is of primary importance to understand their implication in astrophysical environments. For a proper modeling of such processes, it is also required to access quantitative data concerning desorption yields.

The x-ray photodesorption from condensed  $N_2$  and CO has been previously studied for thin layers deposited on top of transition and noble metals (Frigo *et al.*, 1998; Feulner *et al.*, 2000; Romberg *et al.*, 2000; Feulner *et al.*, 2002). In that case, desorption of neutral and ionic molecules ( $N_2$ , CO,  $CO^+$ ) as well as fragments ( $N$ ,  $N^+$ ,  $N^{2+}$ , C, O,  $O^+$ ,  $C^+$ ) was found to strongly depend on singly or multiply valence-excited states, after decay of the core hole state. These states were associated with specific desorption mechanisms. In some cases, ultrafast processes occurring during the core hole state lifetime were also suggested to play a role for the desorption of ionic fragments (Frigo *et al.*, 1998).

For thick molecular ices, characterized by a higher number of layers deposited onto a substrate (generally more than 50 layers), the processes leading to desorption may be different. For instance, after x-ray absorption by molecules in the ice, the relaxation of the core hole state results in the emission of an Auger electron with a probability close to 1 for low  $Z$  elements (Walters and Bhalla, 1971; Krause, 1979). This Auger electron carries most of the initial photon energy and scatters inelastically in the ice, creating secondary events (e.g., ionization and excitation of the surrounding molecules) and, especially, a cascade of secondary low energy ( $<20$  eV) electrons, which may lead to the desorption of molecules from the ice surface. This process is known as x-ray induced electron stimulated desorption (XESD). XESD was not suggested to be the dominant process for the x-ray photodesorption of ions from pure  $N_2$  and CO ice (Feulner *et al.*, 1992; Dupuy *et al.*, 2021b). However, for the desorption of neutrals, it was assumed to be the case for pure CO ice (Dupuy *et al.*, 2021b), pure  $H_2O$  ice (Dupuy *et al.*, 2020), and pure and mixed methanol-containing ices (Basalgète *et al.*, 2021a,b).

Based on quantitative data, x-ray photodesorption of ions from molecular ices is expected to be negligible compared to the desorption of neutrals (Dupuy *et al.*, 2018, 2021b). In the present work, we experimentally study the x-ray photodesorption process for neutral desorption from pure  $^{15}N_2$  ice and from mixed and layered  $^{13}CO:^{15}N_2$  ices (isotopes are chosen to differentiate the molecules by mass spectrometry). Resonant  $1s$  core excitation (or ionization) near the N ( $\sim 400$  eV) or O ( $\sim 500$  eV) K-edge can be achieved thanks to tunable and high spectral resolution x rays from synchrotron facilities, allowing thereby to selectively photoexcite  $^{15}N_2$  or  $^{13}CO$  to trigger desorption from ices containing these molecules. We first provide a quantitative study of the x-ray photodesorption of neutral molecules from pure  $^{15}N_2$  ice. Then, we quantify this process for mixed  $^{13}CO:^{15}N_2$  and layered  $^{13}CO/^{15}N_2$  ( $^{13}CO$  on top of  $^{15}N_2$ ) ices. This latter set of experiments brings important information to discuss the desorption mechanisms.

## II. EXPERIMENT AND METHODOLOGY

### A. Setup and x-ray beamline

To run the experiments, the Surface Processes and ICES (SPICES) setup was connected to the SEXTANTS beamline of the SOLEIL synchrotron facility at Saint-Aubin, France (Sachi *et al.*, 2013). SPICES consists of an ultrahigh vacuum (UHV) chamber (base pressure of  $\sim 10^{-10}$  mbar) at the center of which a copper substrate (polycrystalline oxygen-free high-conductivity copper, surface area of  $1.5 \times 1.5$  cm<sup>2</sup>) can be cooled down to  $\sim 15$  K by a closed-cycle Helium cryostat. The substrate is electrically insulated

from its sample holder by a Kapton foil. This enables the measurement of the drain current generated by electrons escaping the ice after x-ray absorption, which we refer to as the total electron yield (TEY) in the following. The TEY can be measured while scanning the energy of the incident photons and it is representative of the x-ray absorption profile of the ices studied in this work. It is expressed in electrons per incident photon (displayed as  $e^-$  photon<sup>-1</sup> for more simplicity) by correcting the drain current from the photon flux.

The photon flux is measured by a calibrated silicon photodiode mounted on the beamline. The SEXTANTS beamline provides x-ray photons, the energy of which can be finely tuned by means of a monochromator. The energy resolution can also be controlled by adjusting the slit apertures at the exit of the monochromator. In the present study, we have used photons in the 390–460 eV range (nitrogen K-edge) and in the 530–560 eV range (oxygen K-edge). Spectral resolutions of  $\sim 100$  and  $\sim 350$  meV were used to run the experiments. The photon flux varies with the energy and the spectral resolution between  $10^{11}$  and  $10^{12}$  photon s<sup>-1</sup>. The beam was sent at a 47° incidence relative to the normal of the substrate surface and the spot area at the surface was  $\sim 0.1$  cm<sup>2</sup>.

The calibration of the energy scale of the beamline was performed near the N K-edge and the O K-edge as follows:

- Near the N K-edge, the TEY was measured on a pure  $^{15}N_2$  ice as a function of the energy of the incident photons and it was compared to gas phase x-ray absorption spectroscopy experiments (e.g., Chen *et al.*, 1989; Feifel *et al.*, 2004). The TEY peak corresponding to the  $N\ 1s \rightarrow \pi^*$  ( $v' = 0$ ) transition of  $^{15}N_2$  was set to 400.868 eV according to Chen *et al.* (1989) (see Fig. 1 and Sec. III A). We, therefore, assumed that this energy position was not significantly shifted when going from gas phase to solid phase, as observed for a similar molecule: CO (Jugnet *et al.*, 1984). Note that the energy of the transition is slightly varying ( $\pm 20$  meV) from one gas phase experiment to another (King *et al.*, 1977; Hitchcock and Brion, 1980; Sodhi and Brion, 1984; Kempgens *et al.*, 1996; Feifel *et al.*, 2004; Kato *et al.*, 2007).
- Near the O K-edge, the  $O\ 1s \rightarrow \pi^*$  transition of  $^{13}CO$  observed on the TEY of a mixed  $^{13}CO:^{15}N_2$  ice was centered at 534.4 eV (see Fig. 2 and Sec. III A) according to pure CO ice spectroscopy experiments (Jugnet *et al.*, 1984), assuming that the intermolecular interactions between  $^{13}CO$  and  $^{15}N_2$  are not significantly shifting the energy position of the electronic transition, which is reasonable considering such weakly interacting solids.

### B. Ice deposition

Within the SPICES setup, a tube connected to a gas introduction system, which can be translated a few millimeters in front of the substrate surface, enables the injection of a partial pressure of gas phase molecules that stick on the cold surface to form the molecular ices without significantly modifying the base pressure of the UHV chamber. The gaseous molecules used during this work were molecular nitrogen  $^{15}N_2$  (98.6%  $^{15}N$  purity, Eurisotop) and carbon monoxide  $^{13}CO$  (99%  $^{13}C$  purity, Eurisotop). The ice thickness is expressed in monolayer (ML), equivalent to a molecule surface

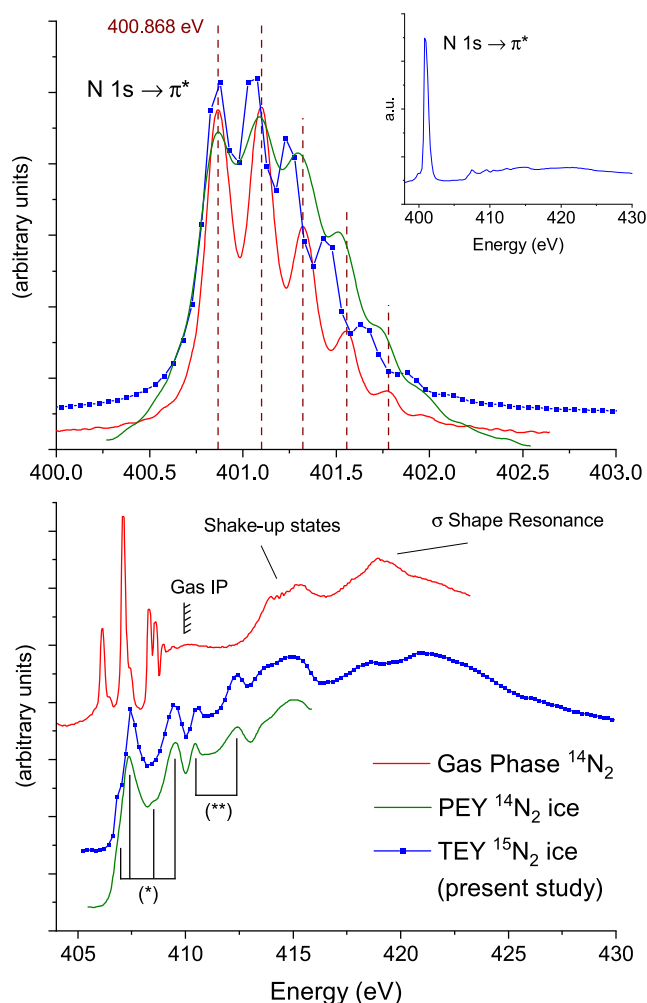


**FIG. 1.** Upper right panel: TEY of  $^{15}\text{N}_2$  ice at 15 K (50 ML) from our experiments in the N K-edge region between 398 and 430 eV. The upper left panel shows the N  $1s \rightarrow \pi^*$  excitation region and the lower panel shows the region near the ionization threshold between 405 and 430 eV. In solid red lines are the x-ray photoabsorption spectra of gas phase  $^{14}\text{N}_2$  from [Chen et al. \(1989\)](#) with a spectral resolution of 40 meV. In solid green lines are the partial electron yields (PEYs) of 50 ML of  $^{14}\text{N}_2$  ice at 15 K from [Feulner et al. \(1992\)](#) with a spectral resolution of 100 meV. In blue lines are the TEYs of 50 ML of  $^{15}\text{N}_2$  ice at 15 K from our experiments with a spectral resolution of 100 meV for the upper left panel and 350 meV for the lower and upper right panels. The baselines of the different curves have been shifted for more clarity. The red dashed vertical lines in the upper left panel are centered on the gas phase vibrational bands.

density of  $\sim 10^{15}$  molecule  $\text{cm}^{-2}$ . Prior to synchrotron experiments, the temperature-programmed desorption (TPD) technique was used to calibrate the rate and deposition time needed to grow a targeted ice thickness. The relative uncertainty on the number of ML deposited during a deposition procedure is about 10% (see, e.g., [Doronin et al., 2015](#)).

The ice samples studied in this work were deposited at 15 K. The mixed  $^{13}\text{CO}:^{15}\text{N}_2$  ices were grown by controlling *in situ* the

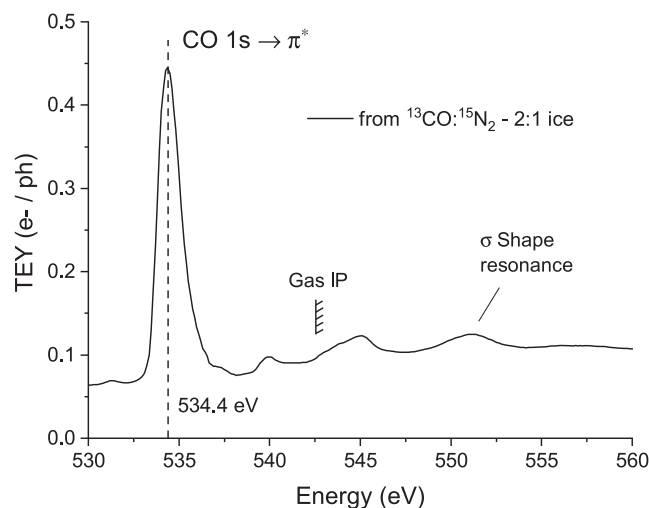


**FIG. 2.** TEY of a mixed  $^{13}\text{CO}:^{15}\text{N}_2$  - 2:1 ice at 15 K (total of 100 ML) in the O K-edge region between 530 and 560 eV from our experiments, with a spectral resolution of 350 meV.

partial pressure of each species injected in the UHV chamber independently (two different valves connected to the deposition tube were used). In this way, the mixing ratio is set by adjusting the partial pressures corresponding to each species. The experiment regarding the layered  $^{13}\text{CO}/^{15}\text{N}_2$  ice (see Sec. III B 3) was achieved by first depositing 50 ML of  $^{15}\text{N}_2$  at 15 K. Then, on top of it, a given number of ML of  $^{13}\text{CO}$  was deposited and the ice was irradiated to measure the photodesorption yields. This operation (deposition of  $^{13}\text{CO}$  on top and irradiation) was sequentially repeated on the same ice until reaching  $\sim 90$  ML of  $^{13}\text{CO}$  on top of the  $^{15}\text{N}_2$  ice. The number of ML of  $^{13}\text{CO}$  deposited at each step is displayed in [Fig. 5](#) (see Sec. III B 3).

### C. Derivation of the photodesorption yields

The photodesorbed molecules are probed in the gas phase during the x-ray irradiation of the ice by means of a quadrupole mass spectrometer (QMS) equipped with an electron impact ionization chamber at 70 eV. The photodesorption of  $^{13}\text{CO}$  and  $^{15}\text{N}_2$  was monitored by recording the QMS signal on the mass channel 29 and 30 u, respectively. The signal intensities are divided by the photon flux and multiplied by a factor  $k$  to obtain the x-ray photodesorption yields  $\Gamma_{raw}$  expressed in molecule desorbed per incident photon (displayed as molecules  $\text{photon}^{-1}$  in the following for more simplicity). The factor  $k$  was derived prior to the synchrotron runs to relate the QMS current to a calibrated number of  $^{15}\text{N}_2$  molecules desorbed during a TPD experiment. For more details on the calibration procedure, see the work of [Basalgète et al. \(2021b\)](#). The apparatus function of our QMS can be considered constant between the mass channels 29 and 30 u and the non-dissociative electron impact ionization cross sections at 70 eV of  $^{13}\text{CO}$  ([Tian and Vidal, 1998](#)) and  $^{15}\text{N}_2$  ([Straub et al., 1996](#)) are nearly equal such that we considered the detection efficiency of our QMS to be similar for  $^{13}\text{CO}$  and  $^{15}\text{N}_2$ . This results in using a similar factor  $k$  for quantifying the photodesorption yields of  $^{13}\text{CO}$  and  $^{15}\text{N}_2$ . The systematic uncertainty

on the photodesorption yields provided by this calibration method is estimated to be ~50%.

In Sec. IV D, we compute the photodesorption yields  $\Gamma_{eV}$  expressed in molecule desorbed per eV deposited by correcting the experimental photodesorption yields  $\Gamma_{raw}$  (expressed in molecules photon<sup>-1</sup>) considering the absorption cross section. This results in the following formula:

$$\Gamma_{eV}(E) = \frac{\Gamma_{raw}(E)}{E a_{dil} (1 - e^{-\sigma(E)N})}, \quad (1)$$

where  $E$  is the energy of the incident photon,  $a_{dil}$  is a factor taking into account the dilution of the photodesorbing molecules in the case of mixed ices (i.e.,  $a_{dil} = 1/3$  and  $2/3$  for the photodesorption yield of, respectively, <sup>15</sup>N<sub>2</sub> and <sup>13</sup>CO from a mixed <sup>13</sup>CO:<sup>15</sup>N<sub>2</sub> – 2:1 ice),  $\sigma(E)$  is the photoabsorption cross section at  $E$ , and  $N$  is the column density involved in the desorption process.  $N$  is equal to  $N = \Lambda_{des} \times b_{dil} \times 10^{15}$  cm<sup>-2</sup>, where  $\Lambda_{des}$  is the desorption-relevant depth expressed in ML (this notion is explained in more detail in Sec. IV), and  $b_{dil}$  is a factor taking into account the dilution of the photoabsorbing molecule in the case of mixed ices (i.e.,  $b_{dil} = 1/3$  and  $2/3$  for the yields derived, respectively, near the N and O K-edge).

### III. RESULTS

#### A. X-ray absorption spectra

##### 1. <sup>15</sup>N<sub>2</sub> ice photoabsorption near N K-edge

The x-ray absorption spectrum of pure <sup>15</sup>N<sub>2</sub> ice at 15 K near the N K-edge, assimilated to our TEY measurements, is displayed in Fig. 1 (blue lines) for different energy ranges and spectral resolutions. The absorption is dominated by the N 1s → π\* transition of <sup>15</sup>N<sub>2</sub> near 401 eV, whose vibrational structure has been resolved with a spectral resolution of 100 meV. Our TEY in the N 1s → π\* region (see upper panel of Fig. 1) compares well with other absorption spectra of gas phase <sup>14</sup>N<sub>2</sub> (Chen *et al.*, 1989) and <sup>14</sup>N<sub>2</sub> ice at 15 K (Feulner *et al.*, 1992). The N 1s<sup>-1</sup>π\* core electronic state of the free molecule is not significantly modified in the solid phase, as expected for weak van der Waals interactions between N<sub>2</sub> molecules in the solid. There are, however, slight discrepancies in the position of the vibrational levels between the three curves in the upper panel of Fig. 1. When going from gas phase (red line) to solid phase (green line), the small differences in the position of the vibrational levels of the N 1s<sup>-1</sup>π\* state of <sup>14</sup>N<sub>2</sub> could be attributed either to experimental uncertainties on the relative position of the peaks or to intermolecular interactions in the solid phase. The comparison of our TEY of <sup>15</sup>N<sub>2</sub> ice (blue line) with the PEY of <sup>14</sup>N<sub>2</sub> ice (green line) shows a smaller vibrational level spacing for <sup>15</sup>N<sub>2</sub>. This is expected to come from an isotopic effect. A similar behavior is observed in the vibrational level spacing of the A<sup>1</sup>Π state of <sup>13</sup>CO vs <sup>12</sup>CO ice and of the b<sup>1</sup>Π<sub>u</sub> state of <sup>15</sup>N<sub>2</sub> vs <sup>14</sup>N<sub>2</sub> ice probed by vacuum ultraviolet (VUV) photodesorption experiments (Bertin *et al.*, 2012; Fayolle *et al.*, 2013). In the lower panel of Fig. 1, the Rydberg states of gas phase <sup>14</sup>N<sub>2</sub> seen below the ionization potential (IP) are significantly modified in the solid phase, as expected from the overlapping of the Rydberg orbitals with that of the neighboring molecules in the solid. Instead, series of broad peaks [labeled (\*)

and (\*\*) in Fig. 1], whose positions go above the gas phase IP, populate this region. There is no significant difference in this region between <sup>14</sup>N<sub>2</sub> and <sup>15</sup>N<sub>2</sub> in the solid phase. The first series of the four peaks labeled (\*) has been attributed to the equivalent of the gas phase Rydberg states 3sσ, 3pπ, 4sσ, and 5sσ in solid phase by Feulner *et al.* (1992), based on polarization dependent x-ray photodesorption of N<sup>+</sup> and based on the data from Chen *et al.* (1989). The attribution of the peaks labeled (\*\*) above the gas phase IP in Fig. 1 has not been studied in the literature to our knowledge. The gas phase broad feature observed near 415 eV has been attributed by Chen *et al.* (1989) to shake-up states, tentatively associated with the state configurations (1s)<sup>-1</sup>(5σ)<sup>-1</sup>(1π<sub>g</sub><sup>\*</sup>)<sup>-1</sup>(3sσ)<sup>-1</sup> and (1s)<sup>-1</sup>(1π)<sup>-1</sup>(1π<sub>g</sub><sup>\*</sup>)<sup>-1</sup>(3pπ)<sup>-1</sup>. As one can see in Fig. 1, a similar feature is observed in this region for <sup>15</sup>N<sub>2</sub> and <sup>14</sup>N<sub>2</sub> ice. The feature observed near 419 eV in the gas phase has been attributed to a σ shape resonance (Chen *et al.*, 1989). A similar feature is observed for <sup>15</sup>N<sub>2</sub> ice.

##### 2. <sup>13</sup>CO:<sup>15</sup>N<sub>2</sub> ice photoabsorption near O K-edge

The TEY of a mixed <sup>13</sup>CO:<sup>15</sup>N<sub>2</sub> ice (2:1) at 15 K near the O K-edge is displayed in Fig. 2. The absorption is dominated by the O 1s → π\* transition of <sup>13</sup>CO centered at 534.4 eV. The spectrum is similar to that of a pure CO ice studied in similar experiments and for which more details are available regarding the attribution of the spectral features (Dupuy *et al.*, 2021b). The intermolecular interactions between <sup>13</sup>CO and <sup>15</sup>N<sub>2</sub> in the mixed ice do not modify the transitions observed in this energy range compared to a pure CO ice. The N 1s core electron photoionization of <sup>15</sup>N<sub>2</sub> is expected to contribute to the absorption spectrum in this energy range, but it is reasonably assumed to be negligible compared to <sup>13</sup>CO photoabsorption, and it should in any case account for a monotonically decreasing signal over the whole energy range.

#### B. X-ray photodesorption yields

##### 1. <sup>15</sup>N<sub>2</sub> pure ice

The photodesorption spectra of <sup>15</sup>N<sub>2</sub> from a pure <sup>15</sup>N<sub>2</sub> ice at 15 K are shown in Fig. 3 (green lines), with the upper panel corresponding to the N 1s → π\* transition and the lower panel corresponding to the near-IP region. The TEYs measured simultaneously during the irradiation procedure are also displayed in blue lines for comparison. The photodesorption yields are higher by more than one order of magnitude in the N 1s → π\* region than in the near-IP region, with a maximum of ~5 molecules photon<sup>-1</sup> at the N 1s → π\* (v' = 0, 1) transitions. The photodesorption spectra follow the same variations as the TEYs except for small discrepancies on the relative intensities of the features, which are likely due to background correction issues and for which we do not attribute any physical meaning. The photodesorption yields of <sup>15</sup>N<sub>2</sub> and the TEYs are obtained from an ice having received a fluence <3.10<sup>16</sup> ph cm<sup>-2</sup>. They both decrease with increasing fluence due to the ice photoaging, that is, the structural and chemical modifications of the ice due to photoabsorption, but the shape of the spectra remains the same and no significant new absorption features are observed in the energy range probed (400–450 eV). The possible photodesorption of <sup>15</sup>N<sub>3</sub> and <sup>15</sup>N<sub>4</sub> was monitored during irradiation, but no desorption signals were found (with a detection limit of

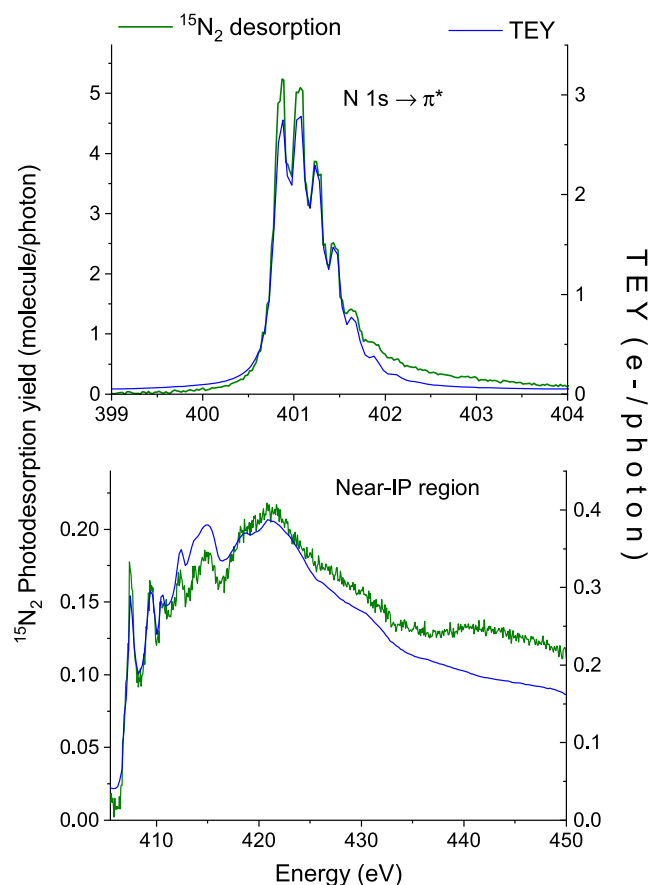


**FIG. 3.** X-ray photodesorption yields of  $^{15}\text{N}_2$  (green lines) from pure  $^{15}\text{N}_2$  ice at 15 K (50 ML) in the  $\text{N } 1s \rightarrow \pi^*$  excitation region (upper panel, spectral resolution of 100 meV) and in the near-IP region (lower panel, spectral resolution of 350 meV). The TEYs measured during the irradiation are also displayed for comparison (in blue lines).

$10^{-2}$  molecules photon $^{-1}$  considering the mass channels and photon flux). Photodesorption of atomic  $^{15}\text{N}$  was only detectable (with a detection limit of  $10^{-3}$  molecules photon $^{-1}$ ) at the  $\text{N } 1s \rightarrow \pi^*$  transition, with a yield of  $\sim 0.01$  molecules photon $^{-1}$ , which is two orders of magnitude less than the desorption yield of  $^{15}\text{N}_2$ .

## 2. Mixed $^{13}\text{CO}:^{15}\text{N}_2$ ice

The photodesorption yields of  $^{13}\text{CO}$  and  $^{15}\text{N}_2$  from mixed  $^{13}\text{CO}:^{15}\text{N}_2$  (2:1 and 20:1) ices are displayed in Fig. 4 in the N K-edge and O K-edge energy range. The TEYs measured simultaneously during the irradiation procedures are also displayed in dashed lines and vertically shifted for more clarity. The shape of the photodesorption spectra is well-correlated to the TEYs both at the N and O K-edge, similar to what is observed for a pure  $^{15}\text{N}_2$  ice. There is, however, a small discrepancy: In the lower panels of Fig. 4, the photodesorption yield of  $^{15}\text{N}_2$  from a mixed  $^{13}\text{CO}:^{15}\text{N}_2$  (2:1) ice is found to decrease after 403 eV for the N K-edge and after 555 eV for the O K-edge whereas the corresponding TEY is constant. This is due to background correction issues.

The photodesorption of  $^{15}\text{N}_2$  from mixed  $^{13}\text{CO}:^{15}\text{N}_2$  ices is found to significantly decrease between the 2:1 and 20:1 ratio at both the N and O K-edges (lower panels of Fig. 4) due to the high dilution of  $^{15}\text{N}_2$ , whereas  $^{13}\text{CO}$  desorption yield is in any case found in the same order of magnitude (upper panels). In the case of a mixed  $^{13}\text{CO}:^{15}\text{N}_2$  (2:1) ice, the photodesorption yields of  $^{13}\text{CO}$  and  $^{15}\text{N}_2$  are found in the same order of magnitude at the  $\text{N } 1s \rightarrow \pi^*$  ( $\sim 1.4 - 1.5$  molecules photon $^{-1}$ ) and the  $\text{O } 1s \rightarrow \pi^*$  ( $\sim 0.5 - 0.7$  molecules photon $^{-1}$ ) transitions of  $^{15}\text{N}_2$  and  $^{13}\text{CO}$ , respectively. This is consistent with the fact that CO and  $\text{N}_2$  have similar binding energies in mixed CO: $\text{N}_2$  ices (Öberg *et al.*, 2005; Bisschop *et al.*, 2006). The fact that the photodesorption yields are lower at the  $\text{O } 1s \rightarrow \pi^*$  transition compared to the  $\text{N } 1s \rightarrow \pi^*$  transition in the case of the 2:1 ratio is probably due to a higher absorption cross section (based on gas phase experiments) of  $^{15}\text{N}_2$  at 401 eV [ $\sim 26$  Mbarn from the work of Kato *et al.* (2007) and when considering the spectral resolution of our photon source] compared to that of  $^{13}\text{CO}$  at 534.4 eV [ $\sim 2.8 - 3.2$  Mbarn from the work of Barrus *et al.* (1979)].

Despite a higher photoabsorption of  $^{13}\text{CO}$  expected for a dilution ratio of 20:1 compared to 2:1, the TEY value at the  $\text{O } 1s \rightarrow \pi^*$  transition of  $^{13}\text{CO}$  is lower for the 20:1 ratio (see right panels of Fig. 4). We would have expected the photodesorption yield of  $^{13}\text{CO}$  to also follow this trend. However, the photodesorption yield of  $^{13}\text{CO}$  at this energy does not change significantly from a 2:1 to a 20:1 ratio (the yield is at  $\sim 0.7$  molecules photon $^{-1}$ ). A higher fluence received by the  $^{13}\text{CO}:^{15}\text{N}_2$  (20:1) ice before this specific measurement seems to be responsible for this behavior. The fluences corresponding to the other measurements displayed in Fig. 4 are similar ( $< 2 \times 10^{16}$  ph cm $^{-2}$ ).

Photodesorption signals were observed on the mass channels 28 u and 44 u. They could correspond to the desorption of  $^{13}\text{C}^{15}\text{N}$  and  $^{13}\text{C}^{15}\text{NO}$ , respectively. However, the signals were too weak ( $\text{S/N} \gtrsim 1$ , with a photodesorption yield of  $\sim 0.02$  molecules photon $^{-1}$  at the  $\text{N } 1s \rightarrow \pi^*$  and the  $\text{O } 1s \rightarrow \pi^*$  for both mass channels) and more easily detected in the case of a 20:1 ratio such that we cannot totally exclude the contribution of  $^{12}\text{CO}$ ,  $^{14}\text{N}_2$  (mass 28 u), and  $^{12}\text{CO}_2$  (mass 44 u) photodesorption to these mass channels due to natural isotopes in our gas samples ( $\sim 1\%$ ). Finally, a desorption signal was found on the mass channel 31 u, which is associated with the x-ray photodesorption of  $^{15}\text{NO}$ . The photodesorption spectra of  $^{15}\text{NO}$  are also following the same variations as the TEYs and the corresponding yields are  $5.3 \times 10^{-2}$  molecules photon $^{-1}$  at the  $\text{N } 1s \rightarrow \pi^*$  transition of  $^{15}\text{N}_2$  and  $2.7 \times 10^{-2}$  molecules photon $^{-1}$  at the  $\text{O } 1s \rightarrow \pi^*$  transition of  $^{13}\text{CO}$  for a  $^{13}\text{CO}:^{15}\text{N}_2$  (2:1) ice. The formation of  $^{15}\text{NO}$  is expected to originate from chemistry induced by the dissociation of  $^{15}\text{N}_2$  and  $^{13}\text{CO}$ . Its presence in the ice has also been evidenced, in very small quantities, by TPD of the photo-irradiated ice at the end of the experiment. The photodesorption yields of the previous photo-products (possibly  $^{13}\text{C}^{15}\text{N}$  and  $^{13}\text{C}^{15}\text{NO}$  for the mass 28 and 44 u, respectively, and unambiguously  $^{15}\text{NO}$  for the mass 31 u) are at least an order of magnitude lower than the yields of  $^{13}\text{CO}$  and  $^{15}\text{N}_2$ . This shows that, if some photochemical change occurs, its impact on the photodesorption process from mixed ices is limited. Photodesorption of atomic  $^{15}\text{N}$ ,  $^{13}\text{C}$ , and O was not detected (with a detection limit of  $10^{-3}$  molecules photon $^{-1}$ ).

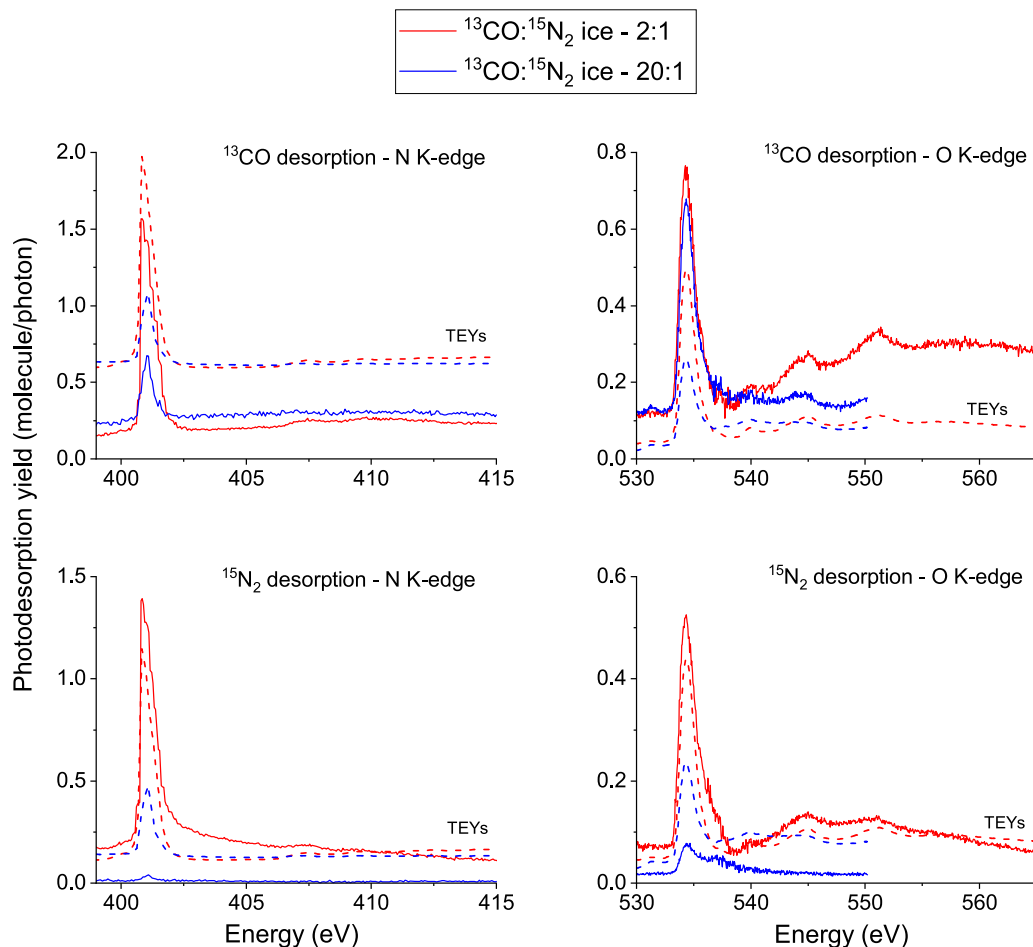


**FIG. 4.** X-ray photodesorption yields of  $^{13}\text{CO}$  and  $^{15}\text{N}_2$  (solid lines) in the N K-edge (left panels) and O K-edge (right panels) regions from mixed  $^{13}\text{CO}:^{15}\text{N}_2$  ices at 15 K (total of 100 ML) with mixing ratio of 2:1 (red lines) and 20:1 (blue lines). The TEYs measured simultaneously during the corresponding irradiation procedure are also displayed in dashed lines in arbitrary units.

### 3. Layered $^{13}\text{CO}/^{15}\text{N}_2$ ice

The photodesorption yields at 401 eV of  $^{13}\text{CO}$  and  $^{15}\text{N}_2$  from a layered  $^{13}\text{CO}/^{15}\text{N}_2$  ice are displayed in Fig. 5 as a function of the number of ML of  $^{13}\text{CO}$  on top of a  $^{15}\text{N}_2$  ice. For this experiment, the photon flux was low ( $\sim 10^{11}$  photon  $\text{s}^{-1}$ ) and the irradiation time was short (a few seconds) in order to ensure that the number of  $^{13}\text{CO}$  molecules photodesorbed during one irradiation step is negligible compared to the number of ML of  $^{13}\text{CO}$  deposited on top of the  $^{15}\text{N}_2$  ice. Considering an x-ray photodesorption yield of  $^{13}\text{CO}$  between 1.0 and 2.4 molecules  $\text{photon}^{-1}$ , an equivalent of 0.01–0.03 ML of  $^{13}\text{CO}$  is desorbed during one irradiation step. In comparison, the first point measured in Fig. 5 is at 1.4 ML of  $^{13}\text{CO}$  on top of the  $^{15}\text{N}_2$  ice. We do not expect significant structural changes of the ice during each irradiation step at such low fluence. Chemical changes are also not expected based on the fact that no signs of significant chemistry are observed on both the TEYs and in desorption for the previous pure and mixed irradiated ices.

At 401 eV, photoabsorption of  $^{15}\text{N}_2$  is due to the  $\text{N } 1s \rightarrow \pi^*$  transition and photoabsorption of  $^{13}\text{CO}$  is due to the ionization of its C 1s electron (IP  $\sim 296$  eV). Quantitatively speaking, and based on gas phase data, the absorption cross section of  $^{15}\text{N}_2$  and  $^{13}\text{CO}$  at 401 eV is  $\sim 20$ – $40$  and  $\sim 0.3$  Mbarn, respectively (Barrus *et al.*, 1979; Kato *et al.*, 2007). Hence, photoabsorption at 401 eV in our layered  $^{13}\text{CO}/^{15}\text{N}_2$  ice is dominated by  $^{15}\text{N}_2$  photoabsorption. The idea of this experiment is, therefore, to trigger the desorption of the above lying  $^{13}\text{CO}$  molecules by photoexcitation of the supporting  $^{15}\text{N}_2$  molecules and to estimate the depth of this indirect desorption mechanism (see Sec. IV) by sequentially depositing monolayers of  $^{13}\text{CO}$  on top of the ice and irradiate it. The contribution of  $^{13}\text{CO}$  photoabsorption to the desorption of  $^{13}\text{CO}$  at 401 eV can be estimated by considering that it is quantitatively similar to the photodesorption of CO from a pure CO ice at 530 eV, which exhibits a photodesorption yield of  $\sim 0.1$  molecules  $\text{photon}^{-1}$  (Dupuy *et al.*, 2021b). This stems from the fact that the photoabsorption of  $^{13}\text{CO}$  at 530 eV is also due to the ionization of its C 1s electron

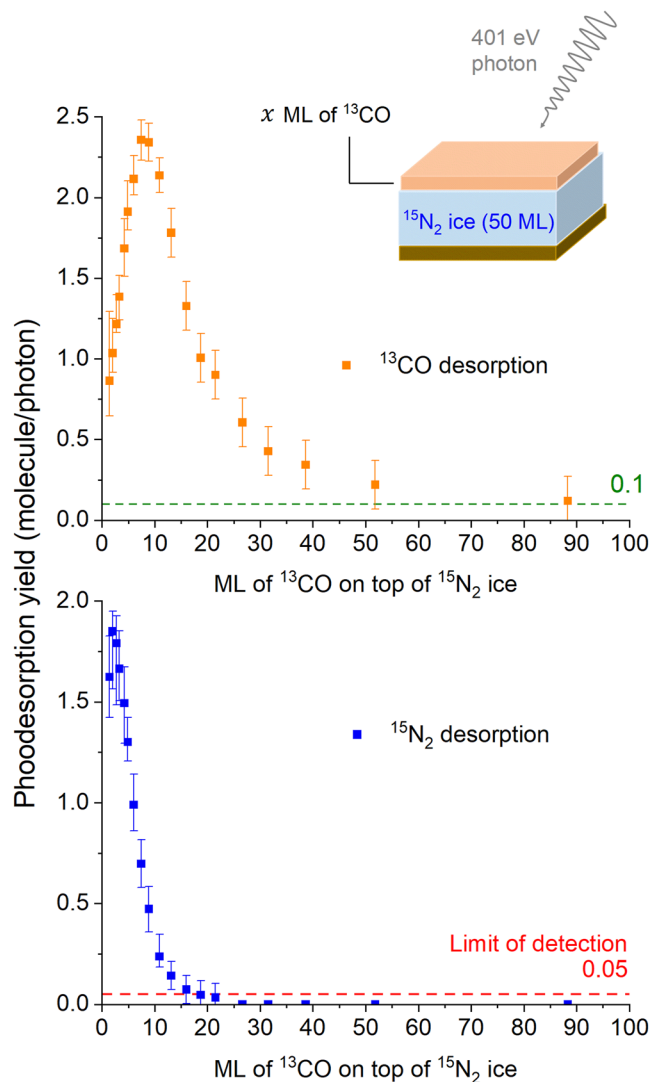


**FIG. 5.** X-ray photodesorption yields at 401 eV of  $^{13}\text{CO}$  (upper panel) and  $^{15}\text{N}_2$  (lower panel) from a layered  $^{13}\text{CO}/^{15}\text{N}_2$  ice at 15 K, as a function of the number of ML of  $^{13}\text{CO}$  deposited on top of a 50 ML  $^{15}\text{N}_2$  ice.

and that we do not expect the ionization cross section to significantly differ between 401 and 530 eV. Consequently, the photodesorption yield of 0.1 molecules photon $^{-1}$  is used as a reference to estimate the contribution of  $^{13}\text{CO}$  photoabsorption to the desorption of  $^{13}\text{CO}$  at 401 eV in our layered ice experiment (it is displayed as a horizontal dashed green line in the upper panel of Fig. 5). From the upper panel of Fig. 5, we observe two different regimes for the photodesorption yield of  $^{13}\text{CO}$ :

- A low to medium coverage regime, for a number of ML of  $^{13}\text{CO}$  from 1 to roughly 30–40 ML: In this regime, the photodesorption yield of  $^{13}\text{CO}$  is  $>0.1$ – $0.2$  molecules photon $^{-1}$  such that the desorption of  $^{13}\text{CO}$  is dominantly triggered

by photoexcitation of  $^{15}\text{N}_2$ . In that case, the photodesorption yield of  $^{13}\text{CO}$  increases until  $\sim 10$  ML and then starts to decrease.

- A high coverage regime, for a number of ML of  $^{13}\text{CO}$   $> 40$  ML: In this regime, the photodesorption yield of  $^{13}\text{CO}$  is close to 0.1 molecules photon $^{-1}$  such that the desorption of  $^{13}\text{CO}$  is dominantly triggered by photoionization of  $^{13}\text{CO}$ . In that case, the possible photodesorption of  $^{13}\text{CO}$  triggered by photoexcitation of  $^{15}\text{N}_2$  can be neglected.

The photodesorption yield of  $^{15}\text{N}_2$  from our layered ice is displayed in the lower panel of Fig. 5. It is found to decrease as the number of ML of  $^{13}\text{CO}$  increases until it goes below our detection limit of  $\sim 0.05$  molecules photon $^{-1}$  (considering the low photon flux for this experiment) for a number of ML of  $^{13}\text{CO}$   $> 15$  ML. The fact that we still observe  $^{15}\text{N}_2$  desorption even when the  $^{15}\text{N}_2$  ice is covered by a few ML of  $^{13}\text{CO}$  may be due to diffusion of  $^{15}\text{N}_2$  from below the ML of  $^{13}\text{CO}$  or due to a few  $^{15}\text{N}_2$  molecules still present at the surface due to inhomogeneous deposition of  $^{13}\text{CO}$ . This is further discussed in Sec. IV C.

## IV. DISCUSSION

### A. Indirect desorption and estimation of $\Lambda_{des}$

Our experiments on mixed  $^{13}\text{CO}/^{15}\text{N}_2$  ices highlight an indirect desorption mechanism, in the sense that the photoabsorption of one molecule is inducing the desorption of another one. This is clearly seen in the mixed  $^{13}\text{CO}/^{15}\text{N}_2$  (2:1) ice for which the photodesorption of  $^{13}\text{CO}$  at the  $^{15}\text{N}_2$  N 1s  $\rightarrow \pi^*$  transition (upper left panel of Fig. 4) and that of  $^{15}\text{N}_2$  at the  $^{13}\text{CO}$  O 1s  $\rightarrow \pi^*$  transition (lower right panel of Fig. 4) dominate the photodesorption spectrum of, respectively,  $^{13}\text{CO}$  and  $^{15}\text{N}_2$ . More globally, the fact that the photodesorption spectrum of  $^{15}\text{N}_2$  and  $^{13}\text{CO}$  follows the x-ray absorption spectrum of, respectively,  $^{13}\text{CO}$  near the O K-edge and  $^{15}\text{N}_2$  near the N K-edge confirms this indirect mechanism. Our experiment on the layered  $^{13}\text{CO}/^{15}\text{N}_2$  ice also sheds light on this process: The ice is irradiated at 401 eV (N 1s  $\rightarrow \pi^*$  transition of  $^{15}\text{N}_2$ ) and  $^{13}\text{CO}$  desorption is observed.

This indirect desorption mechanism necessarily involves energy transport from the molecule that absorbs the incident photon to the molecule that desorbs from the ice surface. The length scale of such energy transport can be defined as the maximum distance from the ice surface (or the depth) at which an absorbed photon can induce desorption. This depth will be defined as  $\Lambda_{des}$  in the following and it will be expressed in ML.  $\Lambda_{des}$  depends on the indirect desorption mechanism and may vary with the photon energy and the ice composition.

Our experiment on the layered  $^{13}\text{CO}/^{15}\text{N}_2$  ice nicely enables the estimation of  $\Lambda_{des}$  for the indirect desorption process of  $^{13}\text{CO}$  induced by the photoabsorption of  $^{15}\text{N}_2$  at 401 eV. In Fig. 5, we can see that  $^{15}\text{N}_2$  photoabsorption can induce  $^{13}\text{CO}$  desorption when the  $^{15}\text{N}_2$  ice is covered by a number of ML of  $^{13}\text{CO}$  from 1 to roughly 30–40 ML, with a maximum efficiency around 10 ML. Above 40 ML, the photodesorption yield of  $^{13}\text{CO}$  from the layered ice is similar to the one induced by the photoionization of the core C 1s electron of  $^{13}\text{CO}$  at 530 eV in pure CO ice (Dupuy *et al.*, 2021b) and the indirect desorption mechanism of  $^{13}\text{CO}$  induced by photoabsorption of  $^{15}\text{N}_2$  is negligible. After fitting, the exponential decay of the

$^{13}\text{CO}$  photodesorption yield starting at  $\sim 10$  ML is associated with a characteristic length of  $\Lambda_c \sim 11$  ML. The exponential reaches 95% extinction at  $3 \times \Lambda_c = 33$  ML, which corresponds to a good estimate of  $\Lambda_{des}$  and for which the indirect desorption of  $^{13}\text{CO}$  becomes negligible. In order to take into account the uncertainty associated with the number of ML of  $^{13}\text{CO}$ , which is  $\sim 10\%$ , we finally estimate that  $\Lambda_{des}$  is between 30 and 40 ML in the case of our layered  $^{13}\text{CO}/^{15}\text{N}_2$  ice and at 401 eV. This shows that desorption can be triggered from the bulk of the ice, beyond the first few ML.

This conclusion can also be drawn for the case of mixed  $^{13}\text{CO}:^{15}\text{N}_2$  ices. In that case, the photodesorption yield of  $^{13}\text{CO}$  at the  $\text{N } 1s \rightarrow \pi^*$  transition of  $^{15}\text{N}_2$  exactly follows the variations of the TEY from a 2:1 to a 20:1 ratio (see upper left panel of Fig. 4). This is not the case for the desorption of  $^{15}\text{N}_2$ , which is barely visible in the case of a 20:1 ratio (see lower left panel of Fig. 4). This could be explained as follows. In the case of the 2:1 ratio,  $^{15}\text{N}_2$  molecules are sufficiently present near the ice surface and within its bulk to observe desorption of both  $^{15}\text{N}_2$  and  $^{13}\text{CO}$  at the  $\text{N } 1s \rightarrow \pi^*$  transition of  $^{15}\text{N}_2$ . However, in the case of the 20:1 ratio,  $^{15}\text{N}_2$  molecules are not sufficiently present near the ice surface to significantly desorb, but they are sufficiently photoabsorbing from the surface to the bulk of the ice to produce a non-negligible TEY value and to induce the desorption of  $^{13}\text{CO}$ . In the case of mixed  $^{13}\text{CO}:^{15}\text{N}_2$  ices, x-ray photodesorption can, therefore, also be triggered from the bulk of the ice.

## B. Indirect desorption mechanisms

In this section, we discuss the possible mechanisms responsible for the indirect desorption of  $^{13}\text{CO}$  by excitation of  $^{15}\text{N}_2$  observed in our layered ice experiment. Extrapolation to the case of the pure and mixed ices will be discussed afterward. One possible mechanism that has been suggested for the x-ray photodesorption of neutrals from ices of simple ( $\text{CO}$ ,  $\text{H}_2\text{O}$ ) and more complex ( $\text{CH}_3\text{OH}$ ) molecules (Dupuy *et al.*, 2018, 2020, 2021b; Basalgète *et al.*, 2021a,b) is x-ray induced electron stimulated desorption (XESD). XESD is a consequence of the relaxation of the core hole photoexcited or photoionized state that decays by emission of an Auger electron with a probability close to 1 for low  $Z$  elements (Walters and Bhalla, 1971; Krause, 1979). This Auger electron scatters inelastically in the ice, creating secondary events (e.g., ionizations and excitations) and a cascade of low energy ( $< 20$  eV) secondary electrons that may lead to desorption.

On the other hand, mechanisms decorrelated from Auger scattering may also play a role. This includes all the mechanisms related to the energy left to the photoabsorbing molecule after Auger decay. Quantitatively, most of the photon energy is given to the Auger electron in the form of kinetic energy ( $\sim 380$  eV for the  $\text{N } 1s \rightarrow \pi^*$  transition of  $^{15}\text{N}_2$ ; Moddemann *et al.*, 1971) and a few tens of eV is left to the photoabsorbing molecule. This latter found itself in a singly or multiply valence-excited state, singly or doubly ionized depending on the energy of the incident photon. For instance, in the specific case of our layered ice experiment at 401 eV,  $^{15}\text{N}_2$  is expected to be left, after Auger decay, in an excited ionized state ( $^{15}\text{N}_2^+)^*$ . The energy left to the molecule in the form of electronic excitation may be transported toward the ice surface via different mechanism to cause indirect desorption (i.e., desorption of other molecules). These mechanisms possibly include the following:

- (1) (a) Indirect desorption due to migration of the electronic excitation through the ice (exciton migration): This mechanism concerns the transport of exciton in ices, a process that stems from the work of Kimmel and co-workers on electron-stimulated desorption (ESD) from  $\text{D}_2\text{O}$  ice (Orlando and Kimmel, 1997; Petrik and Kimmel, 2003). It has also been suggested to play a role in the ESD of  $\text{C}_6\text{H}_6$  on top of water ice by migration of long-lived excitons through the ice (Marchione *et al.*, 2016; Marchione and McCoustra, 2017).
- (b) Relaxation of the excited state to modes coupled with desorption similar to what is observed in VUV photodesorption experiments (Bertin *et al.*, 2013) for which it has been shown that excitation of  $^{13}\text{CO}$  (to the  $\text{A}^1\Pi$  state) and  $^{15}\text{N}_2$  (to the  $\text{b}^1\Pi_u$  state) can induce the desorption of, respectively,  $^{15}\text{N}_2$  and  $^{13}\text{CO}$  from layered ices: In that case, an energy transfer between the excited and the desorbing molecule via excitation of collective vibrational modes (phonons) was suggested. To simplify the following discussion, we will consider that this process occurs without exciton migration, but one should note that it could take place after exciton migration [in that case, it is included in process (1) (a)].
- (2) Indirect desorption due to diffusion of energetic fragments if the ionized excited state is dissociative, similar to the kick-out mechanism suggested in the case of indirect desorption of simple molecules on top of water ice, induced by energetic H atoms that are produced from photodissociation of  $\text{H}_2\text{O}$  in the VUV range (Dupuy *et al.*, 2021a): In some extreme cases, the dissociation may occur before Auger decay.

The aim of our discussion is then to identify the main mechanism responsible for the indirect desorption observed in our layered  $^{13}\text{CO}/^{15}\text{N}_2$  ice experiment. We will especially discriminate between the XESD process and the other processes cited previously that are decorrelated from the Auger scattering and discuss the processes with respect to the value derived for  $\Lambda_{des}$  (30–40 ML).

For a XESD process, the energy absorbed in the bulk of the ice by  $^{15}\text{N}_2$  can be transported toward the ice surface by the scattering of the Auger electron. Considering the energy deposition profile of keV electrons in light materials ( $1 \leq Z \leq 18$ ) from the work of Valkealahti *et al.* (1989), we can reasonably expect that the Auger electron and the secondary electrons can deposit their energy through a few tens of ML. In that sense, the value of  $\Lambda_{des}$  previously estimated (30–40 ML) is consistent with a XESD process. The migration distance of excitons in water ice is potentially tens of ML (Petrik and Kimmel, 2003). Migration of excitons in the case of weakly interacting van der Waals solids such as in  $^{15}\text{N}_2$  ice and migration between  $^{15}\text{N}_2$  and  $^{13}\text{CO}$  layers has not been studied yet, so the process (1)(a) cannot be discussed regarding the value derived for  $\Lambda_{des}$ . However, as discussed in Sec. IV D, we expect this process to depend on the exciton state and, hence, on the incident photon energy.

Process (1) (b) has been characterized by Bertin *et al.* (2013) for the indirect desorption of  $^{13}\text{CO}$  and  $^{15}\text{N}_2$  by excitation of, respectively,  $^{15}\text{N}_2$  and  $^{13}\text{CO}$  in layered ice experiments. In that case, it has been shown that the energy can be efficiently transferred over  $\sim 5$  ML to the desorbing molecules at the surface (this value was similar for excitation of  $^{13}\text{CO}$  to the  $\text{A}^1\Pi$  state and for excitation of  $^{15}\text{N}_2$

to the  $b^1\Pi_u$  state). Therefore, we expect process (1)(b) to be a near-surface process. Process (2) involves the diffusion of ionic or neutral fragments (in that case N or  $N^+$ ) toward the ice surface and collision with  $^{13}\text{CO}$  molecules followed by desorption. After possible dissociation of  $(^{15}\text{N}_2^+)^*$ , we expect the fragments to have less than 10 eV of kinetic energy. Although no studies are available on the typical diffusion length of such fragments in the bulk of molecular ices, we do not expect it to be comparable with the value of  $\Lambda_{des}$  derived. Instead, we expect process (2) to be a near-surface process involving just the first few ML of the ice. This is also supported by the very low level of desorbing  $^{15}\text{N}$  fragments from pure  $^{15}\text{N}_2$  ice (see Sec. III B 1).

Processes (1)(b) and (2) are then expected to possibly occur in the low coverage regime of our layered ice experiment, for a few ML of  $^{13}\text{CO}$  on top of the  $^{15}\text{N}_2$  ice. Regarding the photodesorption yields of  $^{13}\text{CO}$  in Fig. 5, these near-surface processes seem to be negligible compared to the processes involving deeper layers of the  $^{15}\text{N}_2$  ice, such as XESD. In fact, the yields of  $^{13}\text{CO}$  at low coverage (between 1 and 10 ML) and higher coverage are similar. In the low coverage regime, both near-surface processes and bulk processes can participate in indirect desorption, whereas for higher coverage, only

bulk processes participate. The fact that the yields are similar in both regimes excludes a significant contribution of the near-surface processes compared to the bulk ones. Therefore, processes (1)(b) and (2) can be neglected.

In Sec. IV C, we focus on characterizing the XESD process for our layered ice experiment and we conclude on the dominant mechanism expected for indirect desorption of neutral  $^{15}\text{N}_2$  and  $^{13}\text{CO}$  from the ices studied in this work.

### C. Modeling of the energy deposited in the ice by Auger electrons

XESD is mediated by the scattering of Auger electrons. These electrons deposit their energy through the ice via ionization and excitation of the molecules in their path. For a XESD process, the photodesorption yields are expected to be correlated to the amount of energy deposited near the ice surface by the scattering of Auger electrons. This amount of energy can be estimated based on the work of Valkealahti *et al.* (1989). They showed, by Monte Carlo simulations, that the energy deposition profile of a keV electron in a light material ( $1 \leq Z \leq 18$ ) as a function of depth can be approximated

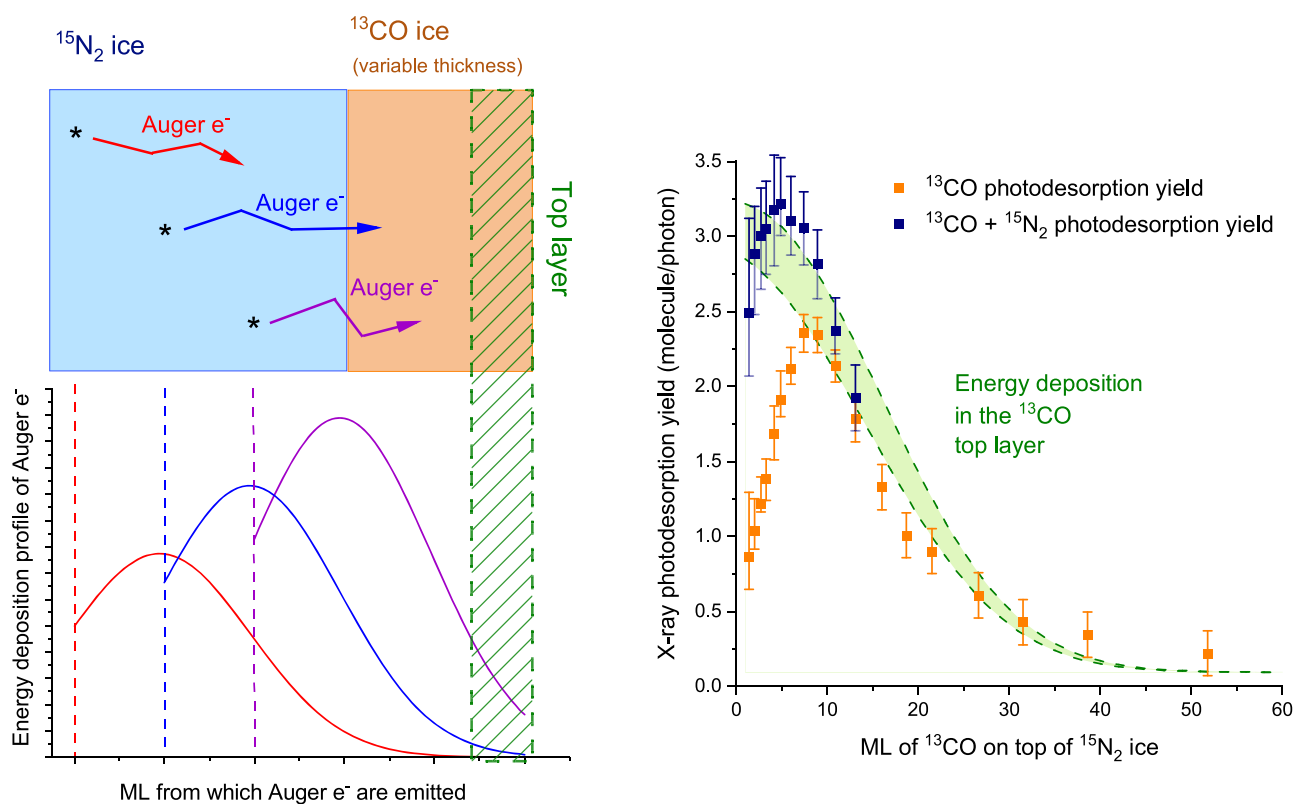


**FIG. 6.** Left side: scheme of our simple model to estimate the energy deposited to the top  $^{13}\text{CO}$  layer of a layered  $^{13}\text{CO}/^{15}\text{N}_2$  ice by scattering of Auger electrons emitted after photoabsorption by  $^{15}\text{N}_2$  molecules. Right side: in green is displayed the estimation of this energy (in arbitrary units and where the zero of the right side distribution has been scaled with a photodesorption yield of  $0.1$  molecules photon $^{-1}$ ), compared with the x-ray photodesorption yields of  $^{13}\text{CO}$  (orange squares) from our layered  $^{13}\text{CO}/^{15}\text{N}_2$  ice (from Fig. 5). The blue squares show the sum of the photodesorption yields of  $^{13}\text{CO}$  plus  $^{15}\text{N}_2$  from our layered  $^{13}\text{CO}/^{15}\text{N}_2$  ice. The upper and lower green curves were computed by taking a photoabsorption cross section at 401 eV of 40 and 20 Mbarn, respectively.

by a Gaussian distribution (in 1D). The parameters of the distribution depend on the energy of the electron and on the stopping power of the material at this energy. These parameters have been fitted for a  $\text{N}_2$  ice. We can, therefore, estimate the amount of energy deposited near the ice surface by the scattering of Auger electrons in the case of our layered  $^{13}\text{CO}/^{15}\text{N}_2$  ice experiment using the following methodology and assumptions (this is also sketched in the left side of Fig. 6):

- We consider a layered  $^{13}\text{CO}/^{15}\text{N}_2$  ice: 50 ML of  $^{15}\text{N}_2$  on top of which an increasing number of ML of  $^{13}\text{CO}$  is deposited. We neglect the photoabsorption of the  $^{13}\text{CO}$  layers at 401 eV.
- We assume that the initial kinetic energy of the Auger electron emitted by relaxation of the  $\text{N}(1s)^{-1}\pi^*$  state of  $^{15}\text{N}_2$  is  $\sim 380$  eV, based on Auger spectra of gas phase  $\text{N}_2$  (Moddeman *et al.*, 1971).
- We only consider the emitted Auger electrons that statistically contribute the most to the energy deposited near the ice surface, i.e., the Auger electrons that are emitted from the bulk toward the surface of the ice.
- The energy deposition profile of the Auger electrons is approximated by a Gaussian distribution with parameters from Valkealahti *et al.* (1989), in 1D. This also takes into account the energy loss of secondary electrons and it is computed as the sum of the average kinetic energy of all electrons in a depth element. According to the Born–Bethe approximation and Bragg’s rule, the stopping power of  $^{13}\text{CO}$  and  $^{15}\text{N}_2$  at 380 eV is similar, so we reasonably assumed that the energy deposition profile does not significantly differ in  $^{15}\text{N}_2$  or  $^{13}\text{CO}$  layers. The shape of the energy deposition profiles is plotted in arbitrary units in the left panel of Fig. 6.
- We consider that each ML of  $^{15}\text{N}_2$  is emitting a number of Auger electrons that are equal to the number of photons absorbed in that ML. Thus, the relative intensity of the energy deposition distributions from two different ML is driven by a Beer–Lambert law, with an absorption cross section at 401 eV taken between 20 and 40 Mbarn (Kato *et al.*, 2007).

The energy deposited in the top layer of the  $^{13}\text{CO}$  ice is then computed by summing the contributions from each ML of  $^{15}\text{N}_2$ . This operation is repeated for an increasing number of ML of  $^{13}\text{CO}$  deposited on top of the  $^{15}\text{N}_2$  ice. The results are presented in the right panel of Fig. 6: The energy deposited on the top layer of the  $^{13}\text{CO}$  ice is compared to the experimental photodesorption yields of  $^{13}\text{CO}$  from our layered  $^{13}\text{CO}/^{15}\text{N}_2$  ice (taken from Fig. 5). A comparison with the sum of the photodesorption yields of  $^{13}\text{CO}$  plus  $^{15}\text{N}_2$ , which have similar photodesorption yields at 401 eV when mixed in similar stoichiometries (according to our results from mixed ices), is also done for the following discussion. At low coverage (number of ML of  $^{13}\text{CO} \lesssim 10$  ML), the ice surface is not homogeneously covered by  $^{13}\text{CO}$  molecules and the photodesorption yield of  $^{13}\text{CO}$  increases linearly with the number of  $^{13}\text{CO}$  molecules available for desorption. Therefore, in this regime, the photodesorption yield of  $^{13}\text{CO}$  is not correlated with the energy deposition of Auger electrons since it actually depends on the ice surface homogeneity. This lack of homogeneity is supported by the fact that  $^{15}\text{N}_2$  still desorbs in

this regime. Furthermore, in this low coverage regime, we observe a good agreement between the energy deposition profile and the sum of the photodesorption yields of  $^{13}\text{CO}$  plus  $^{15}\text{N}_2$  (see blue squares in Fig. 6). This is consistent with the ice surface being composed of a mix of  $^{13}\text{CO}$  and  $^{15}\text{N}_2$  molecules in the low coverage regime and for which photodesorption of neutral molecules is correlated with the energy deposited at the top layer and dominated by  $^{13}\text{CO}$  plus  $^{15}\text{N}_2$  desorption (no significant desorption is found for other possible neutral molecules). For medium coverage (number of ML of  $^{13}\text{CO}$  between 10 and 40 ML), the exponential decay of the  $^{13}\text{CO}$  desorption yield is in good agreement with the modeled deposited energy. For high coverage (number of ML of  $^{13}\text{CO} > 40$  ML), the photodesorption is triggered by the photoionization of  $^{13}\text{CO}$  (see Sec. III B 3).

These results strongly suggest that XESD is the dominant mechanism responsible for the indirect desorption of  $^{13}\text{CO}$  at 401 eV from our layered  $^{13}\text{CO}/^{15}\text{N}_2$  ice. It also confirms our estimated value for  $\Lambda_{des}$ . In that case, excitation of  $^{13}\text{CO}$  to non-dissociative states by low energy secondary electrons (produced by the Auger scattering) may be the exact mechanism explaining  $^{13}\text{CO}$  desorption. For comparison, ESD of CO from pure CO ice has an energy threshold around 6 eV (Rakhovskaia *et al.*, 1995), which is accessible to the secondary electrons, as suggested in Dupuy *et al.* (2021b). This energy threshold is around 7 eV for the ESD of  $\text{N}_2$  from pure  $\text{N}_2$  ice.

Auger emission occurs with a probability close to one for each core hole state of  $^{15}\text{N}_2$  or  $^{13}\text{CO}$  above and below their respective IP. The energy deposition profile due to the Auger scattering is also reasonably expected to be similar in the different ices tested in this work (pure  $^{15}\text{N}_2$  ice, mixed  $^{13}\text{CO}:^{15}\text{N}_2$  ices, and layered  $^{13}\text{CO}/^{15}\text{N}_2$  ice), based on the fact that  $^{13}\text{CO}$  and  $^{15}\text{N}_2$  have similar stopping power in the energy range considered. It is, therefore, straightforward to consider that XESD should also play a role in the desorption of  $^{15}\text{N}_2$  from pure  $^{15}\text{N}_2$  ice and in the desorption of  $^{13}\text{CO}$  and  $^{15}\text{N}_2$  from mixed  $^{13}\text{CO}:^{15}\text{N}_2$  ices, at each photon energy. The simple model previously implemented nicely enables the estimation of  $\Lambda_{des}$  for a XESD process at different photon energies as long as the photoabsorption cross section and the initial kinetic energy of the Auger electron emitted after core hole decay are known. This is used in Sec. IV D.

#### D. Conversion of the absorbed energy to desorption

In this section, we correct our x-ray photodesorption yields by taking into account only the part of the absorbed energy that can participate in the desorption process. This results in expressing the yields in molecules  $(\text{eV deposited})^{-1}$  using Eq. (1). We consider that the number of the top monolayers involved in the desorption process ( $\Lambda_{des}$ ) should be at least equal to the one corresponding to a XESD process. The energy absorbed in the layers beyond  $\Lambda_{des}$  is “lost” in the sense that it cannot be converted to desorption. This results in taking  $\Lambda_{des} = 30\text{--}40$  ML near the N K-edge, where the photoabsorption is dominated by  $^{15}\text{N}_2$  absorption. Near the O K-edge, the photoabsorption is dominated by  $^{13}\text{CO}$  absorption and the Auger electron is expected to have an initial kinetic energy between 500 and 520 eV (Moddeman *et al.*, 1971). Based on our simple modeling in Sec. IV C, this results in a slightly higher  $\Lambda_{des}$  (40–50 ML). The results are presented in Table I (first four rows) for

**TABLE I.** Photodesorption yields expressed in molecule desorbed by eV deposited, of  $^{13}\text{CO}$  and  $^{15}\text{N}_2$  from different ices and at different energies, computed via Eq. (1) and by using the experimental yields derived in this work. The lower and higher values of the yields are derived by taking the higher and lower value of  $\Lambda_{des}$ , respectively.

Photon energy	$\sigma$ (Mbarn) <sup>a</sup>	$\Lambda_{des}$ (ML)	Photodesorption yield [ $\times 10^{-2}$ molecules (eV deposited) <sup>-1</sup> ]			
			$^{15}\text{N}_2$ from		$^{13}\text{CO}$ from	
			Pure $^{15}\text{N}_2$	$^{13}\text{CO}:^{15}\text{N}_2$ (2:1)	Pure $^{13}\text{CO}$	$^{13}\text{CO}:^{15}\text{N}_2$ (2:1)
401 eV ( $^{15}\text{N}_2$ ; N 1s $\rightarrow \pi^b$ )	26	30–40	1.9–2.3	3.2–4.1		1.9–2.5
425 eV ( $^{15}\text{N}_2$ ; N 1s ionization)	1.8	30–40	0.6–0.8	<sup>b</sup>		2.1–2.8
534.2 eV ( $^{13}\text{CO}$ ; O 1s $\rightarrow \pi^b$ )	3.0	40–50		2.8–3.5		2.1–2.6
570 eV ( $^{13}\text{CO}$ ; O 1s ionization)	0.8	40–50		<sup>b</sup>	1.5 <sup>c</sup>	2.4–3.0
8.3 eV [ $^{13}\text{CO}$ ; $A^1\Pi - X^1\Sigma^+ (2,0)$ ] <sup>d</sup>	15	5		18	8.3	21

<sup>a</sup>The photoabsorption cross section is taken from gas phase measurements (Barrus et al., 1979; Kato et al., 2007) and we took into account the spectral resolution of our photon source.

<sup>b</sup>Background issues on the mass channel 30 around 425 eV and 570 eV during the x-ray irradiation of the  $^{13}\text{CO}:^{15}\text{N}_2$  2:1 ice prevent us from using the experimental yields of  $^{15}\text{N}_2$  at these energies.

<sup>c</sup>Taken from Dupuy et al. (2021b) where it was assumed that  $\Lambda_{des} = 30$  ML.

<sup>d</sup>From Bertin et al. (2013).

the desorption of  $^{13}\text{CO}$  and  $^{15}\text{N}_2$  from their respective pure ice and from mixed  $^{13}\text{CO}:^{15}\text{N}_2$  (2:1) ices at different photon energies.

The yields displayed in Table I represent a quantitative estimate of how efficiently the absorbed energy (only the part that can participate in the desorption process) is converted to the desorption channel. This takes into account all the desorption processes that may occur due to photoabsorption in the first  $\Lambda_{des}$  ML of the ice. The estimated yields are very similar for the desorption of  $^{13}\text{CO}$  and  $^{15}\text{N}_2$  from pure or mixed ices and at each energy considered. They range between  $\sim 0.02$  and  $\sim 0.04$  molecules (eV deposited)<sup>-1</sup>. There is, however, a small discrepancy with the photodesorption yield of  $^{15}\text{N}_2$  from pure  $^{15}\text{N}_2$  ice at 425 eV, which is lower than the previous values. This is assumed to be due to a higher fluence received by the ice before this specific measurement compared to the other ones.

These results indicate that there is presumably a unique dominant process explaining the desorption of  $^{13}\text{CO}$  and  $^{15}\text{N}_2$  from the ices tested and whose efficiency does not strongly depend on the photon energy; hence, it depends neither on the photoabsorbing molecule nor on its state after Auger decay (singly or doubly ionized excited state). This is fully consistent with a XESD process for which desorption depends only on the Auger scattering, the latter being expected to not significantly differ between pure and mixed ices of  $^{13}\text{CO}$  and  $^{15}\text{N}_2$ . The similarity of the yields between  $^{13}\text{CO}$  and  $^{15}\text{N}_2$  is also consistent with their similar binding energies in pure or mixed ice (Öberg et al., 2005; Bisschop et al., 2006). A possible significant desorption due to exciton migration from the photoabsorbing molecule (process (1)(a) defined in Sec. IV B) can also be excluded by the fact that the efficiency of this process is expected to depend on the exciton state after Auger decay and, therefore, on the photon energy, which is not what we observe in Table I.

Finally, in Table I, we also computed the VUV photodesorption yields in molecules (eV deposited)<sup>-1</sup> at 8.3 eV, which corresponds to the  $A^1\Pi - X^1\Sigma^+ (2,0)$  electronic transition of  $^{13}\text{CO}$ , from the data published in Bertin et al. (2013). In this study,  $\Lambda_{des}$  was estimated to be  $\sim 5$  ML for the indirect desorption mechanism from layered

$^{15}\text{N}_2/^{13}\text{CO}$  experiments. The yields in molecules (eV deposited)<sup>-1</sup> are found higher in the VUV range (at 8.3 eV) than in the x-ray range. This means that the energy absorbed by a valence excitation of  $^{13}\text{CO}$  (to the  $A^1\Pi$  state) is more efficiently converted to desorption, by a process similar to the one described in Sec. IV B [process (1)(b)], than the energy absorbed by a core hole excitation or ionization (of  $^{13}\text{CO}$  or  $^{15}\text{N}_2$ ) and for which a XESD process is expected to be dominant according to our results. This is true for both the VUV photodesorption of  $^{13}\text{CO}$  (direct and/or indirect process) and  $^{15}\text{N}_2$  (indirect process) from pure  $^{13}\text{CO}$  ice and mixed  $^{13}\text{CO}:^{15}\text{N}_2$  ice.

## V. CONCLUSION

X-ray photodesorption of  $^{15}\text{N}_2$  from pure  $^{15}\text{N}_2$  ice and of  $^{15}\text{N}_2$  and  $^{13}\text{CO}$  from mixed  $^{13}\text{CO}:^{15}\text{N}_2$  ices is found to follow the x-ray absorption profile of the ices in the N and O K-edge energy range (near 400 and 500 eV, respectively). Photodesorption experiments on mixed  $^{13}\text{CO}:^{15}\text{N}_2$  ices revealed an indirect desorption mechanism triggered by the absorption of  $^{15}\text{N}_2$  near the N K-edge and  $^{13}\text{CO}$  near the O K-edge, leading to both  $^{13}\text{CO}$  and  $^{15}\text{N}_2$  desorption. This indirect mechanism is also highlighted by the desorption of  $^{13}\text{CO}$  from an x-ray irradiated layered  $^{13}\text{CO}/^{15}\text{N}_2$  ice at 401 eV. This latter experiment enables the derivation of the relevant depth of desorption  $\Lambda_{des}$ , which is a quantitative measure of depth involved in the indirect desorption process. It was estimated to be 30–40 ML near the N K-edge. The photodesorption yields of  $^{13}\text{CO}$  from the layered  $^{13}\text{CO}/^{15}\text{N}_2$  ice as a function of  $^{13}\text{CO}$  coverage are found to be well-correlated to the amount of energy deposited at the top layer by the scattering of Auger electrons after x-ray absorption, the latter being estimated by a simple model based on the work of Valkealahti, Schou, and Nieminen (1989). The desorption yields of  $^{13}\text{CO}$  and  $^{15}\text{N}_2$  corrected from the absorbed energy that can participate in desorption do not significantly depend on the photon energy (hence on the photoabsorbing molecule,  $^{13}\text{CO}$  or  $^{15}\text{N}_2$ ) and on the nature of the ice (pure or mixed). These results indicate that

XESD, mediated by the scattering of Auger electrons, is the dominant mechanism explaining the x-ray photodesorption of  $^{15}\text{N}_2$  and  $^{13}\text{CO}$  from the ices tested in this work.

## ACKNOWLEDGMENTS

This work was carried out with financial support from the Region Ile-de-France DIM-ACAV + program; the Sorbonne Université “Emergence” program; the ANR PIXyES project, Grant No. ANR-20-CE30-0018 of the French “Agence Nationale de la Recherche”; and the Program National “Physique et Chimie du Milieu Interstellaire” (PCMI) of CNRS/INSU with INC/INP co-funded by CEA and CNES. We would like to acknowledge SOLEIL for the provision of synchrotron radiation facilities under Project No. 20210142 and N. Jaouen, H. Popescu, and R. Gaudemer for their help on the SEXTANTS beamline.

## AUTHOR DECLARATIONS

### Conflict of Interest

The authors have no conflicts to disclose.

### Author Contributions

**R. Basalgète:** Data curation (equal); Formal analysis (equal); Methodology (equal); Writing – original draft (lead); Writing – review & editing (equal). **M. Bertin:** Formal analysis (equal); Writing – review & editing (equal). **D. Torres-Díaz:** Formal analysis (equal); Writing – review & editing (equal). **A. Lafosse:** Formal analysis (equal); Writing – review & editing (equal). **L. Amiaud:** Formal analysis (equal); Writing – review & editing (equal). **G. Féraud:** Formal analysis (equal); Writing – review & editing (equal). **P. Jeseck:** Formal analysis (equal); Writing – review & editing (equal). **L. Philippe:** Formal analysis (equal); Writing – review & editing (equal). **X. Michaut:** Formal analysis (equal); Writing – review & editing (equal). **J.-H. Fillion:** Formal analysis (equal); Writing – review & editing (equal).

## DATA AVAILABILITY

The data that support the findings of this study are available within the article.

## REFERENCES

- Barrus, D. M., Blake, R. L., Burek, A. J., Chambers, K. C., and Pregoner, A. L., “K-shell photoabsorption coefficients of  $\text{O}_2$ ,  $\text{CO}_2$ ,  $\text{CO}$ , and  $\text{N}_2\text{O}$ ,” *Phys. Rev. A* **20**, 1045–1061 (1979).
- Basalgète, R., Dupuy, R., Féraud, G., Romanzin, C., Philippe, L., Michaut, X., Michoud, J., Amiaud, L., Lafosse, A., Fillion, J.-H., and Bertin, M., “Complex organic molecules in protoplanetary disks: X-ray photodesorption from methanol-containing ices. I. Pure methanol ices,” *Astron. Astrophys.* **647**, A35 (2021a).
- Basalgète, R., Dupuy, R., Féraud, G., Romanzin, C., Philippe, L., Michaut, X., Michoud, J., Amiaud, L., Lafosse, A., Fillion, J.-H., and Bertin, M., “Complex organic molecules in protoplanetary disks: X-ray photodesorption from methanol-containing ices. II. Mixed methanol-CO and methanol- $\text{H}_2\text{O}$  ices,” *Astron. Astrophys.* **647**, A36 (2021b).
- Bennett, C. J., Pirim, C., and Orlando, T. M., “Space-weathering of solar system bodies: A laboratory perspective,” *Chem. Rev.* **113**, 9086–9150 (2013).
- Bertin, M., Fayolle, E. C., Romanzin, C., Öberg, K. I., Michaut, X., Moudens, A., Philippe, L., Jeseck, P., Linnartz, H., and Fillion, J.-H., “UV photodesorption of interstellar CO ice analogues: From subsurface excitation to surface desorption,” *Phys. Chem. Chem. Phys.* **14**, 9929 (2012).
- Bertin, M., Fayolle, E. C., Romanzin, C., Poderoso, H. A. M., Michaut, X., Philippe, L., Jeseck, P., Öberg, K. I., Linnartz, H., and Fillion, J.-H., “Indirect ultraviolet photodesorption from  $\text{CO:N}_2$  binary ices — An efficient grain-gas process,” *Astrophys. J.* **779**, 120 (2013).
- Bisschop, S. E., Fraser, H. J., Öberg, K. I., van Dishoeck, E. F., and Schlemmer, S., “Desorption rates and sticking coefficients for CO and  $\text{N}_2$  interstellar ices,” *Astron. Astrophys.* **449**, 1297–1309 (2006).
- Boogert, A. C. A., Gerakines, P. A., and Whittet, D. C. B., “Observations of the icy universe,” *Annu. Rev. Astron. Astrophys.* **53**, 541–581 (2015).
- Chen, C. T., Ma, Y., and Sette, F., “K-shell photoabsorption of the  $\text{N}_2$  molecule,” *Phys. Rev. A* **40**, 6737–6740 (1989).
- Ciaravella, A., Muñoz Caro, G. M., Jiménez-Escobar, A., Cecchi-Pestellini, C., Hsiao, L. C., Huang, C. H., and Chen, Y. J., “X-ray processing of a realistic ice mantle can explain the gas abundances in protoplanetary disks,” *Proc. Natl. Acad. Sci. U. S. A.* **117**, 016149 (2020).
- Cruikshank, D. P., Roush, T. L., Owen, T. C., Geballe, T. R., de Bergh, C., Schmitt, B., Brown, R. H., and Bartholomew, M. J., “Ices on the surface of triton,” *Science* **261**, 742–745 (1993).
- Doronin, M., Bertin, M., Michaut, X., Philippe, L., and Fillion, J.-H., “Adsorption energies and prefactor determination for  $\text{CH}_3\text{OH}$  adsorption on graphite,” *J. Chem. Phys.* **143**, 084703 (2015).
- Dupuy, R., Bertin, M., Féraud, G., Hassenfratz, M., Michaut, X., Putaud, T., Philippe, L., Jeseck, P., Angelucci, M., Cimino, R., Baglin, V., Romanzin, C., and Fillion, J.-H., “X-ray photodesorption from water ice in protoplanetary disks and x-ray-dominated regions,” *Nat. Astron.* **2**, 796–801 (2018).
- Dupuy, R., Bertin, M., Féraud, G., Michaut, X., Marie-Jeanne, P., Jeseck, P., Philippe, L., Baglin, V., Cimino, R., Romanzin, C., and Fillion, J.-H., “Mechanism of indirect photon-induced desorption at the water ice surface,” *Phys. Rev. Lett.* **126**, 156001 (2021a).
- Dupuy, R., Bertin, M., Féraud, G., Romanzin, C., Putaud, T., Philippe, L., Michaut, X., Jeseck, P., Cimino, R., Baglin, V., and Fillion, J.-H., “X-ray induced desorption and photochemistry in CO ice,” *Phys. Chem. Chem. Phys.* **23**, 15965–15979 (2021b).
- Dupuy, R., Féraud, G., Bertin, M., Romanzin, C., Philippe, L., Putaud, T., Michaut, X., Cimino, R., Baglin, V., and Fillion, J.-H., “Desorption of neutrals, cations, and anions from core-excited amorphous solid water,” *J. Chem. Phys.* **152**, 054711 (2020).
- Fayolle, E. C., Bertin, M., Romanzin, C., Michaut, X., Öberg, K. I., Linnartz, H., and Fillion, J.-H., “CO ice photodesorption: A wavelength-dependent study,” *Astrophys. J.* **739**, L36 (2011).
- Fayolle, E. C., Bertin, M., Romanzin, C., Poderoso, H. A. M., Philippe, L., Michaut, X., Jeseck, P., Linnartz, H., Öberg, K. I., and Fillion, J.-H., “Wavelength-dependent UV photodesorption of pure  $\text{N}_2$  and  $\text{O}_2$  ices,” *Astron. Astrophys.* **556**, A122 (2013).
- Feifel, R., Andersson, M., Öhrwall, G., Sorensen, S. L., Piancastelli, M. N., Tchapyguine, M., Björneholm, O., Karlsson, L., and Svensson, S., “A quantitative analysis of the  $\text{N } 1s \rightarrow \pi^*$  photoabsorption profile in  $\text{N}_2$ : New spectroscopical constants for the core-excited state,” *Chem. Phys. Lett.* **383**, 222–229 (2004).
- Feulner, P., Ecker, M., Romberg, R., Weimar, R., and Föhlisch, A., “Core-excitation-induced bond breaking of chemisorbed molecules probed by emission of ions, neutrals, and electrons,” *Surf. Rev. Lett.* **09**, 759–768 (2002).
- Feulner, P., Romberg, R., Frigo, S. P., Weimar, R., Gsell, M., Ogurtsov, A., and Menzel, D., “Recent progress in the investigation of core hole-induced photon stimulated desorption from adsorbates: Excitation site-dependent bond breaking, and charge rearrangement,” *Surf. Sci.* **451**, 41–52 (2000).
- Feulner, P., Scheuerer, R., Scheuer, M., Remmers, G., Wurth, W., and Menzel, D., “High resolution photon stimulated desorption spectroscopy of solid nitrogen by resonant N 1s core level excitation,” *Appl. Phys. A: Mater. Sci. Process* **55**, 478–481 (1992).

- Frigo, S. P., Feulner, P., Kassühlke, B., Keller, C., and Menzel, D., "Observation of neutral atomic fragments for specific 1s core excitations of an adsorbed molecule," *Phys. Rev. Lett.* **80**, 2813–2816 (1998).
- Hitchcock, A. P. and Brion, C. E., "K-shell excitation spectra of CO, N<sub>2</sub> and O<sub>2</sub>," *J. Electron Spectrosc. Relat. Phenom.* **18**, 1–21 (1980).
- Jiménez-Escobar, A., Ciaravella, A., Cecchi-Pestellini, C., Huang, C.-H., Sie, N.-E., Chen, Y.-J., and Muñoz Caro, G. M., "X-ray photo-desorption of H<sub>2</sub>O:CO:NH<sub>3</sub> circumstellar ice analogs: Gas-phase enrichment," *Astrophys. J.* **868**, 73 (2018).
- Jugnet, Y., Himpfel, F. J., Avouris, P., and Koch, E. E., "High-resolution C 1s and O 1s core-excitation spectroscopy of chemisorbed, physisorbed, and free CO," *Phys. Rev. Lett.* **53**, 198–201 (1984).
- Kato, M., Morishita, Y., Oura, M., Yamaoka, H., Tamenori, Y., Okada, K., Matsudo, T., Gejo, T., Suzuki, I. H., and Saito, N., "Absolute photoionization cross sections with ultra-high energy resolution for Ar, Kr, Xe and N<sub>2</sub> in inner-shell ionization regions," *J. Electron Spectrosc. Relat. Phenom.* **160**, 39–48 (2007).
- Kempgens, B., Kivimäki, A., Neeb, M., Köppe, H. M., Bradshaw, A. M., and Feldhaus, J., "A high-resolution N 1s photoionization study of the N<sub>2</sub> molecule in the near-threshold region," *J. Phys. B: At., Mol. Opt. Phys.* **29**, 5389–5402 (1996).
- King, G. C., Read, F. H., and Tronc, M., "Investigation of the energy and vibrational structure of the inner shell (1s)<sup>-1</sup>(π2p)<sup>1</sup>π state of the nitrogen molecule by electron impact with high resolution," *Chem. Phys. Lett.* **52**, 50–54 (1977).
- Krause, M. O., "Atomic radiative and radiationless yields for K and L shells," *J. Phys. Chem. Ref. Data* **8**, 307–327 (1979).
- Marchione, D. and McCoustra, M. R. S., "Electron-induced chemistry: Preliminary comparative studies of hydrogen production from water, methanol, and diethyl ether," *ACS Earth Space Chem.* **1**, 310–315 (2017).
- Marchione, D., Thrower, J. D., and McCoustra, M. R. S., "Efficient electron-promoted desorption of benzene from water ice surfaces," *Phys. Chem. Chem. Phys.* **18**, 4026–4034 (2016).
- Moddeman, W. E., Carlson, T. A., Krause, M. O., Pullen, B. P., Bull, W. E., and Schweitzer, G. K., "Determination of the K-LL Auger spectra of N<sub>2</sub>, O<sub>2</sub>, CO, NO, H<sub>2</sub>O, and CO<sub>2</sub>," *J. Chem. Phys.* **55**, 2317–2336 (1971).
- Mumma, M. J. and Charnley, S. B., "The chemical composition of comets—Emerging taxonomies and natal heritage," *Annu. Rev. Astron. Astrophys.* **49**, 471–524 (2011).
- Muñoz Caro, G. M., Jiménez-Escobar, A., Martín-Gago, J. Á., Rogero, C., Atienza, C., Puertas, S., Sobrado, J. M., and Torres-Redondo, J., "New results on thermal and photodesorption of CO ice using the novel InterStellar Astrochemistry Chamber (ISAC)," *Astron. Astrophys.* **522**, A108 (2010).
- Öberg, K. I., Fuchs, G. W., Awad, Z., Fraser, H. J., Schlemmer, S., van Dishoeck, E. F., and Linnartz, H., "Photodesorption of CO ice," *Astrophys. J.* **662**, L23–L26 (2007).
- Öberg, K. I., van Broekhuizen, F., Fraser, H. J., Bisschop, S. E., van Dishoeck, E. F., and Schlemmer, S., "Competition between CO and N<sub>2</sub> desorption from interstellar ices," *Astrophys. J.* **621**, L33–L36 (2005).
- Öberg, K. I., van Dishoeck, E. F., and Linnartz, H., "Photodesorption of ices I: CO, N<sub>2</sub>, and CO<sub>2</sub>," *Astron. Astrophys.* **496**, 281–293 (2009).
- Orlando, T. M. and Kimmel, G. A., "The role of excitons and substrate temperature in low-energy (5–50 eV) electron-stimulated dissociation of amorphous D<sub>2</sub>O ice," *Surf. Sci.* **390**, 79–85 (1997).
- Owen, T. C., Roush, T. L., Cruikshank, D. P., Elliot, J. L., Young, L. A., de Bergh, C., Schmitt, B., Geballe, T. R., Brown, R. H., and Bartholomew, M. J., "Surface ices and the atmospheric composition of Pluto," *Science* **261**, 745–748 (1993).
- Petrik, N. G. and Kimmel, G. A., "Electron-stimulated reactions at the interfaces of amorphous solid water films driven by long-range energy transfer from the bulk," *Phys. Rev. Lett.* **90**, 166102 (2003).
- Rakhovskaya, O., Wiethoff, P., and Feulner, P., "Thresholds for electron stimulated desorption of neutral molecules from solid N<sub>2</sub>, CO, O<sub>2</sub> and NO," *Nucl. Instrum. Methods Phys. Res., Sect. B* **101**, 169–173 (1995).
- Romberg, R., Heckmair, N., Frigo, S. P., Ogurtsov, A., Menzel, D., and Feulner, P., "Atom-selective bond breaking in a chemisorbed homonuclear molecule induced by core excitation: N<sub>2</sub>/Ru (001)," *Phys. Rev. Lett.* **84**, 374–377 (2000).
- Rubin, M., Altwegg, K., Balsiger, H., Bar-Nun, A., Berthelier, J.-J., Bieler, A., Bochsler, P., Briois, C., Calmonte, U., Combi, M., De Keyser, J., Dhooche, F., Eberhardt, P., Fiethe, B., Fuselier, S. A., Gasc, S., Gombosi, T. I., Hansen, K. C., Hässig, M., Jäckel, A., Kopp, E., Korth, A., Le Roy, L., Mall, U., Marty, B., Mousis, O., Owen, T., Rème, H., Sémon, T., Tzou, C.-Y., Waite, J. H., and Wurz, P., "Molecular nitrogen in comet 67P/Churyumov-Gerasimenko indicates a low formation temperature," *Science* **348**, 232–235 (2015).
- Sacchi, M., Jaouen, N., Popescu, H., Gaudemer, R., Tonnerre, J. M., Chiuzbaian, S. G., Hague, C. F., Delmotte, A., Dubuisson, J. M., Cauchon, G., Lagarde, B., and Polack, F., "The SEXTANTS beamline at SOLEIL: A new facility for elastic, inelastic and coherent scattering of soft x-rays," *J. Phys.: Conf. Ser.* **425**, 072018 (2013).
- Sodhi, R. N. S. and Brion, C. E., "Reference energies for inner shell electron energy-loss spectroscopy," *J. Electron Spectrosc. Relat. Phenom.* **34**, 363–372 (1984).
- Straub, H. C., Renault, P., Lindsay, B. G., Smith, K. A., and Stebbings, R. F., "Absolute partial cross sections for electron-impact ionization of H<sub>2</sub>, N<sub>2</sub>, and O<sub>2</sub> from threshold to 1000 eV," *Phys. Rev. A* **54**, 2146–2153 (1996).
- Tian, C. and Vidal, C. R., "Cross sections of the electron impact dissociative ionization of CO, CH<sub>4</sub> and C<sub>2</sub>H<sub>2</sub>," *J. Phys. B: At., Mol. Opt. Phys.* **31**, 895–909 (1998).
- Valkealahti, S., Schou, J., and Nieminen, R. M., "Energy deposition of keV electrons in light elements," *J. Appl. Phys.* **65**, 2258–2266 (1989).
- Walters, D. L. and Bhalla, C. P., "Nonrelativistic auger rates, x-ray rates, and fluorescence yields for the K shell," *Phys. Rev. A* **3**, 1919–1927 (1971).